IEEE Access
Multidisciplinary ⋮ Rapid Review ⋮ Open Access Journal

Received 4 August 2023, accepted 7 September 2023, date of publication 14 September 2023,
date of current version 25 September 2023.

Digital Object Identifier 10.1109/ACCESS.2023.3315590

RESEARCH ARTICLE

Dynamic Optimization of Rotor-Side PI Controller Parameters for Doubly-Fed Wind Turbines Based on Improved Recurrent Neural Networks Under Wind Speed Fluctuations

TAO CHENG[1], JIAHUI WU[1], HAIYUN WANG[1], AND HONGJUAN ZHENG[2]
[1]State Centre for Engineering Research, Ministry of Education for Renewable Energy Generation and Grid-Connected Control, Xinjiang University, Urumqi 830047, China
[2]Guodian Nanrui Technology Company Ltd., Nanjing, Jiangsu 211106, China

Corresponding author: Jiahui Wu (wjh229@xju.edu.cn)

This work was supported in part by the Open Project of Key Laboratory in Xinjiang Uygur Autonomous Region of China under Grant 2023D04071, and in part by the National Natural Science Foundation of China under Grant 52167016.

ABSTRACT This paper investigates a doubly-fed wind turbine generation system (DFIG) where the rotor-side control parameters have a significant impact on the effectiveness of the DFIG due to the adoption of its inner-loop current and outer-loop power control strategies. Under rated operation, the original DFIG parameter adjustment relies mainly on manual adjustment. In this paper, mathematical models are established through literature research and data search, and neural networks are found to have unique advantages in dynamic automatic parameter tuning. First, a mathematical model of DFIG based on PI controller is established in this paper, and then the improved recurrent neural network is applied to the parameter tuning control of rotor-side PI controller, and an experimental model of DFIG simulation based on the improved recurrent neural network is established in MATLAB/Simulink. By comparing the DFIG models before and after the improvement, the simulation experiments verify that the DFIG system based on the improved recurrent neural network (CLR-DRNN) has significant control advantages under the wind speed fluctuation. The simulation experimental results show that the DFIG system based on the improved recurrent neural network achieves significant improvement in wind energy utilization coefficient, active power, reactive power, response time of rotor speed, overshoot and static error compared with the conventional PI-regulated DFIG system.

INDEX TERMS PI controller, double-fed wind turbine (DFIG), diagonal recurrent neural network (DRNN), wind power generation (WF).

I. INTRODUCTION

Wind energy is a renewable energy source that reduces dependence on traditional fossil fuels, reduces greenhouse gas emissions, and protects the environment. Wind turbines are the primary means of harnessing wind energy, which is based on the principle that the rotation of a wind turbine drives a generator to generate electricity. Wind energy has become an important renewable energy source worldwide due to its abundant resources, non-pollution, renewable nature and cost effectiveness [1]. At present, wind energy is widely used in the fields of power generation, heating, and hydrogen production, and the future applications are promising.

Wind power systems can be divided into constant speed constant frequency (CSCF) and variable speed constant frequency (VSCF) systems, which depend on the operation of the turbine [2]. In CSCF systems, the generator maintains a constant rotor speed and operates at a constant frequency,

The associate editor coordinating the review of this manuscript and approving it for publication was Tariq Masood.

while VSCF systems allow variable speed operation by controlling the voltage frequency of the rotor. Compared to CSCF systems, VSCF systems have a higher wind energy utilization.

A notable representative of the VSCF system is the doubly-fed induction generator (DFIG). Compared to other types of generators, the DFIG exhibits higher efficiency, flexibility and adaptability. Its rotor can be controlled to adapt to different wind speeds and load variations. Moreover, since only 25-30% of the rated power is converted and the rest is transmitted directly to the grid, DFIG wind turbines minimize costs, power losses, and converter size, making them more affordable than other types of turbines [4].

The key component to operate and control a DFIG-based wind power system is the dual pulse width modulation (PWM) converter. The converter consists of a grid-side converter (GSC) and a rotor-side controller (RSC). The GSC stabilizes the bus voltage of the DC link and ensures operation at unit power factor, while the RSC plays an important role in achieving variable speed, constant frequency generation and maximizing wind energy tracking.

To maintain optimal generator operation, it is critical to develop an effective excitation control strategy for the DFIG's RSC. Decoupling simplifies the design and composition of the controller and promotes a wide range of flexible regulation and control of the DFIG. Proportional-integral (PI) control is commonly used in controllers due to its simplicity, fast response time, and satisfactory performance in terms of accuracy and stability.

In DFIG-based wind power systems, optimization of the PI parameters of the RSC is critical to ensure that the rotor angular velocity closely tracks the optimal velocity corresponding to the current wind speed, thereby increasing the wind energy conversion rate and improving the control performance of the RSC [5]. Although manual adjustment of control parameters based on the DFIG linearization model can be performed under specific operating conditions, it may lead to degradation of control performance when the operating conditions change. There are two main problems with this approach [6]. First, the calculation of PI controller parameters is dependent on the system settings, making the control susceptible to errors due to factors such as temperature rise, equipment damage, grid faults, or any other changes, which may lead to dynamic response oscillations, instability, or negative effects on system performance. Secondly, there is a lack of adaptive capability to external disturbances [7].

To address these problems, scholars have proposed partial solutions for the PI controller of DFIG wind power systems. Some researchers sought reliable and effective methods to tune the optimal PI control parameters based on various operating conditions. Since finding the optimal PI controller parameters involves an optimization problem, some scholars have utilized mathematical optimization methods that rely mainly on gradient information, such as Newton's method and interior point method [8]. However, these methods rely on the accuracy and precision of the system model and cannot be dynamically updated in real time, which may prevent the DFIG wind power system from obtaining the optimal control parameters. Other researchers have proposed alternative solutions and used intelligent optimization algorithms to dynamically seek the best PI parameter scheme in real time for optimal control of DFIG.

Intelligent optimization algorithms provide a general search strategy for optimization and are not limited to a specific environment. They offer various optimization advantages, including model-independent, expert experience-independent, derivative-free mechanisms, and avoidance of local optimization [9]. Therefore, intelligent optimization algorithms can be applied to optimize the PI parameters of RSCs. Well-known algorithms in this regard include genetic algorithms (GA), ant colony optimization algorithms (WOA), and particle swarm optimization algorithms (PSO) [10]. These algorithms simulate the natural behavior of animals, such as movement and predation, in order to find the best solution. However, traditional intelligent algorithms face challenges in optimizing the control parameters of RSC due to large search space, limited global and local search capabilities, lack of diversity, and long optimization time.

To overcome these limitations, researchers have focused on two mainstream intelligent algorithms for optimizing PI control of DFIG wind power systems: fuzzy logic algorithms and neural network algorithms [12].

Fuzzy logic control is a control technique that deals with fuzzy or uncertain information through imprecise reasoning rather than precise computation [13]. It involves fuzzy inference with variable values between 0 and 1 rather than strict 0 or 1 [14]. Neural network control is a control system inspired by the human nervous system [15]. It mimics the structure and function of the human brain [16] and uses the exchange of information between artificial neurons to determine the input signals. Neural network control is effective in managing continuous, nonlinear and multivariable systems.

Fuzzy logic control is based on predetermined rules and information processing, whereas neural network control relies on learning and training among neurons to make decisions. However, fuzzy logic control also has some limitations [17]. Adjusting system parameters and fuzzy rules can be time-consuming, and these parameters and rules may vary from case to case. Fuzzy logic control is limited by the fuzzy language, and it is difficult to compare fuzzy quantities and sets with other mathematical concepts. This limitation limits the accuracy and scope of control [18], [19].

Compared to fuzzy logic control, neural network control exhibits greater learning and adaptation capabilities [20], [21]. It can adapt to changes in the internal and external environment of the system through learning and training to achieve more accurate control. In contrast, fuzzy logic control relies on predefined fuzzy rules and cannot learn and adapt autonomously. Second, [22] neural network control can handle more complex processing tasks. It can solve nonlinear, non-smooth and highly noisy control problems, providing higher flexibility and applicability. On the other

hand, fuzzy logic control is more suitable for simpler, linear and low-noise control problems. Third, [23] neural networks possess greater robustness, [24] and neural network control can adapt and self-heal, automatically correcting problems caused by noise and disturbances, thus improving resilience. In contrast, fuzzy logic control is relatively less tolerant of noise and disturbances. In conclusion, compared with fuzzy logic control, neural network control shows stronger advantages in terms of adaptability, flexibility and robustness.

Neural networks are mainly classified into two categories: feedforward neural networks (FNN) and recurrent neural networks (RNN) [25]. Feedforward neural networks are the basic type of neural networks and consist of an input layer, multiple hidden layers, and an output layer. The neurons within each layer are fully interconnected [26]. In FNNs, data can only flow towards the front, hence the name feedforward neural network. On the other hand, RNNs incorporate a memory function and include recursive connections [27].

The advantages of FNNs are their relatively fast training speed, their ability to handle inputs of different lengths [28], and their good performance for simple classification problems. However, FNNs are not suitable for time-series data or data with internal dependencies and struggle to handle long-term dependencies [29]. Complex classification problems require more hidden layers and neurons, resulting in larger models, which is a challenge for training.

In contrast, RNNNs outperform FNNNs [30] in handling time-series data and data with internal dependencies. With its memory function, RNNs can handle long-term dependencies and perform well in sequential modeling tasks such as speech recognition and natural language processing. However, RNNs also have some drawbacks [31], including a slow training speed and the possibility of gradient disappearance or explosion due to the presence of internal recursive connections, which makes the training process more difficult.

In response to the above problems, some scholars have proposed relevant solutions. In a study [32], a combination of neural network and sliding mode control was designed to improve the parameter adaptation and immunity to disturbances of a pneumatic actuator controller. The neural network was used to observe the uncertainty of the whole system. Another study [33] used BP neural networks in combination with PI control methods for speed control of a permanent magnet synchronous motor in an elevator, resulting in improved speed and comfort. Another study [34] proposed a decoupled control strategy for permanent magnet synchronous motors, which combines classical proportional-integral-derivative (PID) control with a single neuron. This approach promotes the decoupled control of the motor with fast response capability and good static performance. The connection weight parameter plays a key role in tuning the performance of PID neural networks (PIDNN) for complex control systems. In another study [35], an MPIDNN method based on adaptive population extremum optimization, namely PEO-MPIDNN, was proposed for optimizing the control problem of multivariate nonlinear control systems. Simulation results show that the proposed PEO-MPIDNN has superior transient, steady-state, and robust control performance compared with other methods.

In addition, a study [36] proposed an adaptive control method based on artificial neural networks for a wind energy conversion system (WECS) using doubly-fed asynchronous generators (DFIG). Numerical simulations showed that the power of the DFIG system was significantly improved by the proposed control scheme compared to vector and sliding mode control techniques. Another study [37] focused on the analysis and design of a hybrid control (HC) system for a doubly-fed asynchronous generator (DFIG) using a recurrent neural network (RNN) and a proportional-integral (PI) controller. The proposed hybrid controller exhibits fast dynamics and good transient response to sudden changes in wind speed and generator speed.

To improve the control performance of DFIG systems, this paper explores the use of diagonal recurrent neural networks (DRNN) in combination with PI control [38].The dynamic properties of DRNN allow for effective control of nonlinear time-varying systems. In this approach, the DRNN adjusts the optimal parameters of the PI in real time during the system operation, and an adaptive learning rate method is designed to improve the learning ability and online correction capability of the controller. Simulation experiments confirm that the improved CLR-DRNN-PI control method enhances the responsiveness and anti-disturbance capability of the DFIG speed loop, thus improving the static and dynamic performance of the whole DFIG system. The following points highlight the contributions of this study:

1. conventional PI control, BP neural network-based PI control, and DRNN diagonal recurrent neural network-based PI control are compared and analyzed.
2. the learning rate of the DRNN algorithm is optimized.
3. Combined PI controller and DRNN for doubly-fed wind turbine to achieve faster convergence speed.
4. A mathematical model and simulation model of the DFIG system were developed, and Simulink simulations were performed using a 2 MW DFIG wind turbine to verify the effectiveness of the proposed control method.
5. Finally, the evaluation was carried out based on the power convergence, wind energy utilization factor and rotor speed.

In this paper, we propose an improved diagonal recurrent neural network to overcome the problems of too large search space, weak global search ability and weak local search ability of traditional intelligent algorithms in optimizing the PI parameters of RSC. The parameters of the PI controller are tuned by building an improved diagonal recurrent neural network (DRNN). the DRNN approach provides better response time, minimizes overshoot, and maintains adequate tracking of the reference under wind speed variation conditions.

II. DFIG MODELING AND VECTOR CONTROL

The grid-connected DFIG model is shown in Figure 1. It contains a wind turbine, a doubly-fed induction generator (DFIG), an inverter commonly referred to as a back-to-back power electronic converter (also called an inverter-side converter), and a control system. Both inverters are connected to a DC-link capacitor. the stator side of the DFIG is connected to the grid via a coupling transformer. Where RSC is the rotor-side converter and GSC is the stator-side converter.

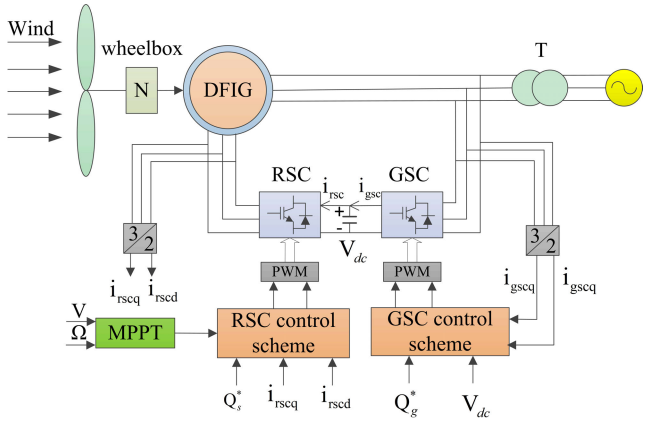

FIGURE 1. Grid-connected DFIG-WT model.

A. WORKING PRINCIPLE OF WIND POWER MAXIMUM POWER POINT TRACKING (MPPT) AND DFIG WIND TURBINE

The grid-connected DFIG model is shown in Figure 1. It contains a wind turbine, a doubly-fed induction generator (DFIG), an inverter commonly referred to as a back-to-back power electronic converter (also called an inverter-side converter), and a control system. Both inverters are connected to a DC-link capacitor. the stator side of the DFIG is connected to the grid via a coupling transformer. Where RSC is the rotor-side converter and GSC is the stator-side converter.

According to the aerodynamic characteristics of the wind turbine, the input power of the wind turbine is:

$$P_v = \frac{1}{2}(\rho S_w v)\, v^2 = \frac{1}{2}\rho S_w v^3 \tag{1}$$

where ρ is the air density, under standard conditions, $\rho = 1.293 kg/m^3$, S_w is the windward sweeping area of the wind blade, v is the wind speed.

Since the wind energy absorbed by the wind turbine is only a fraction of the wind energy flowing through the wind turbine, the wind energy utilization factor C_p is usually defined to represent the efficiency of wind energy captured by the wind turbine, C_p is:

$$C_p = \frac{P_o}{P_v} \tag{2}$$

Then the output power P_o of the wind turbine in equation (2) can be expressed as:

$$P_o = C_p P_v = \frac{1}{2}\rho S_w v^3 C_p = \frac{\pi}{2}\rho R_w^2 v^3 C_p \tag{3}$$

where R_w is the radius of the airfoil.

The leaf tip speed ratio λ is an important concept in the wind turbine modeling process, which is the ratio of the linear speed of the wind blade tip to the ratio of wind speed:

$$\lambda = \frac{R_w \omega_w}{v} = \frac{\pi R_w n_w}{30 v} \tag{4}$$

where ω_w is the angular velocity of wind blade rotation, n_w is the wind blade speed, and when $n_w = \frac{30\omega_w}{\pi}$, the output torque T of the wind turbine can be expressed as:

$$T_o = \frac{P_o}{\omega_w} = \frac{\pi \rho R_w^3 v^2 C_p}{2\lambda} \tag{5}$$

According to the Baez theory, the wind energy utilization coefficient C_p is a composite function of the variables of the blade tip speed ratio λ and the pitch angle β, which is expressed as:

$$\begin{aligned} C_p(\lambda, \beta) &= 0.5176\left(\frac{116}{\lambda_i} - 0.4\beta - 5\right) e^{-\frac{21}{\lambda_i}} + 0.0068\lambda \\ \frac{1}{\lambda_i} &= \frac{1}{\lambda + 0.08\beta} - \frac{0.035}{\beta^3 + 1} \end{aligned} \tag{6}$$

where: λ_i can be represented by λ and β.

The expression for the optimal power curve is:

$$\begin{aligned} P_{opt} &= \frac{\pi}{2}\rho R_w^2 v^3 C_{p\max} \\ P_{opt} &= \frac{\pi}{2}\rho R_w^2 \left(\frac{R_w}{\lambda_{opt}}\right)^3 C_{p\max}\omega_w^3 = k\omega_w^3 \end{aligned} \tag{7}$$

where: $k = \frac{\pi}{2}\rho R_w^2 \left(\frac{R_w}{\lambda_{opt}}\right)^3 C_{p\max}$

Then, as the wind speed changes, adjusting the wind turbine speed to keep it at the optimal speed position will enable the wind turbine to work continuously on the optimal power curve and achieve the maximum wind energy tracking.

Let the number of pole pairs of the motor be P, the frequency of the stator output current be f_s, which is also equal to the grid frequency, the rotor excitation current - the frequency of the three-phase AC current flowing into the rotor windings be f_r, the rotational speed of the motor rotor be n, the rotational speed of the stator rotating magnetic field be n_s, and the rotor rotating magnetic field relative to the rotor be n_r. Then:

$$n_s = \frac{60 f_s}{p}, \quad n_r = \frac{60 f_r}{p} \tag{8}$$

The transfer rates are:

$$s = \frac{(n_s - n)}{n_s} \tag{9}$$

$$n + n_r = n_s \tag{10}$$

From the derivation of equations (8), (9) and (10), the following relationship can be obtained:

$$f_r = \frac{p n_r}{60} = \frac{(n_s - n)}{n_s}\frac{p n_s}{60} = s f_s \tag{11}$$

According to equation (11), as the wind speed changes, the speed n of the doubly-fed wind turbine will also change.

In order to keep the frequency f_s constant at the grid frequency, a three-phase AC current of frequency $f_r = sf_s$ needs to be fed to the rotor winding. Therefore, only when the rotor excitation current has a frequency $f_r = sf_s$, the doubly-fed wind turbine can be operated at a constant frequency. The expression for the electromagnetic torque a of a doubly-fed wind turbine is:

$$T_e = \frac{3}{2} p L_m \left(i_{sd} i_{rq} - i_{sq} i_{rd}\right) \tag{12}$$

where p is the number of motor pole pairs.

Equation of motion:

$$T_e - T_l = \frac{J}{p}\frac{d\omega_r}{dt} + \frac{D}{p}\omega_r + \frac{K}{p}\theta_r \tag{13}$$

where T_l is the driving torque of the motor; J is the rotational inertia of the motor; ω_r is the electrical angular velocity of the rotor winding as the rotor rotates; D is the torque damping coefficient of the motor; and K is the torsional elastic torque coefficient of the motor. Equations (12) to (16) form the mathematical model of the doubly-fed wind turbine in a three-phase stationary coordinate system.

B. PARK CONVERTER CONTROL

The rotor-side converter mainly realizes decoupling control of the output active and reactive power. The three-phase coordinate system is transferred to the rotating reference coordinate system (dq-reference coordinate system) by the Park transform.

Thus, the stator and rotor voltage equations are expressed as follows:

$$\begin{cases} \mathrm{U_{sd}} = -\mathrm{R}_s \mathrm{i_{sd}} + \dfrac{\mathrm{d}\psi_{\mathrm{sd}}}{\mathrm{dt}} - \omega_1 \psi_{\mathrm{sq}} \\ \mathrm{U_{sq}} = -\mathrm{R}_s \mathrm{i_{sq}} + \dfrac{\mathrm{d}\psi_{\mathrm{sq}}}{\mathrm{dt}} + \omega_1 \psi_{\mathrm{sd}} \end{cases} \tag{14}$$

$$\begin{cases} \mathrm{U_{rd}} = \mathrm{R_r i_{rd}} + \dfrac{\mathrm{d}\psi_{\mathrm{rd}}}{\mathrm{dt}} - \omega_s \psi_{\mathrm{rq}} \\ \mathrm{U_{rq}} = \mathrm{R_r i_{rq}} + \dfrac{\mathrm{d}\psi_{\mathrm{rq}}}{\mathrm{dt}} + \omega_s \psi_{\mathrm{rd}} \end{cases} \tag{15}$$

Generator stator and rotor winding magnetic chain equation:

$$\begin{cases} \psi_{\mathrm{sd}} = L_s \mathrm{i_{sd}} - L_m \mathrm{i_{rd}} \\ \psi_{\mathrm{sq}} = L_s \mathrm{i_{sq}} - L_m \mathrm{i_{rq}} \end{cases} \tag{16}$$

$$\begin{cases} \psi_{\mathrm{rd}} = L_r \mathrm{i_{rd}} - L_m \mathrm{i_{sd}} \\ \psi_{\mathrm{rq}} = L_r \mathrm{i_{rq}} - L_m \mathrm{i_{sq}} \end{cases} \tag{17}$$

The electromagnetic torque is shown below:

$$T_{\mathrm{e}} = \frac{3}{2} p L_m (i_{sd} i_{rq} - i_{sq} i_{rd}) \tag{18}$$

The stator active and reactive power is written as follows:

$$\begin{cases} P_{\mathrm{s}} = \dfrac{3}{2}(U_{sd} i_{sd} + U_{sq} i_{sq}) \\ \mathrm{Q_s} = \dfrac{3}{2}(U_{sq} i_{sd} - U_{sd} i_{sq}) \end{cases} \tag{19}$$

C. RSC CONVERTER CONTROL

Indirect vector control is used to individually regulate the power of the generator and solve the coupling problem of the system. The power is controlled in the open loop, while the closed loop is used to control the rotor current. The stator flux is assumed to be constant and oriented in the d-axis. Due to the elimination of the stator winding resistance, the rotor voltage can be expressed as:

$$\begin{cases} u_{rd} = R_r i_{rd} + \sigma \dfrac{di_{rd}}{dt} - \omega_s \sigma i_{rq} \\ u_{rq} = R_r i_{rq} + \sigma \dfrac{di_{r\omega}}{dt} + \omega_s \sigma i_{rd} + \omega_s \dfrac{L_m}{L_s} \psi_s \end{cases} \tag{20}$$

In order to simplify the control system and improve the control accuracy, the decoupling term of the rotor voltage and the feed-forward compensation term can be decomposed, where the feed-forward decoupling terms u'_{rd} and u'_{rq} of the rotor voltage are:

$$\begin{cases} u'_{rd} = R_r i_{rd} + \sigma \dfrac{di_{rd}}{dt} \\ u'_{rq} = R_r i_{rq} + \sigma \dfrac{di_{rq}}{dt} \end{cases} \tag{21}$$

The rotor d-axis voltage decoupling term u'_{rd} is only affected by the rotor d-axis current i_{rd}, and the rotor q-axis voltage decoupling term u'_{rq} is only affected by the rotor d-axis current i_{rq}, which is equivalent to the completion of the decoupling of rotor d- and q-axis currents. In addition, the feedforward compensation terms Δu_{rd} and Δu_{rq} for the rotor voltage are:

$$\begin{cases} \Delta u_{rd} = -\omega_s \sigma i_{rq} \\ \Delta u_{rq} = \omega_s \sigma i_{rd} + \omega_s \dfrac{L_m}{L_s} \psi_s \end{cases} \tag{22}$$

We have the expressions for the stator active and reactive power expressed by the rotor d and q axis currents as follows:

$$\begin{cases} P_s = \dfrac{3}{2} u_s \dfrac{L_m}{L_s} i_{rq} \\ Q_s = \dfrac{3}{2} u_s \left(\dfrac{L_m}{L_s} i_{rd} - \dfrac{1}{L_s} \psi_s\right) \end{cases} \tag{23}$$

When the grid is stable and the stator magnetic chain is oriented, it can be considered that ψ_s is a constant value, and according to equation (23), the stator active power P_s and reactive power Q_s are determined by the rotor d and q axis currents i_{rq} and i_{rd}, respectively, which is equivalent to having achieved power decoupling.

The expression for the electromagnetic torque T_e of the doubly-fed wind turbine is then as follows:

$$T_e = -\frac{3}{2} p \frac{L_m}{L_s} \psi_s i_{rq} \tag{24}$$

Since ψ_s can be considered as a constant value, according to equation (24), the electromagnetic torque T_e of the doubly-fed wind turbine can also be controlled by the rotor d and q axis current i_{rq}. According to the relationship between electromagnetic torque and rotational speed, the rotational

speed of the doubly-fed wind turbine can also be controlled by the rotor d and q axis currents i_{rq}.

The pole compensation method is used to calculate the PI coefficient (K_{pr}, K_{Ir}). The time constants of the system are:

$$K_s = \left(L_r - \frac{L_m^2}{L_s}\right)/R \tag{25}$$

Therefore, the expression for the PI coefficient is calculated as follows:

$$\begin{cases} K_{pr} = \dfrac{1}{K_r}\left(L_r - \dfrac{L_m^2}{L_s}\right) \\ K_{Ir} = \dfrac{K_{pr} R_r}{\left(L_r - \frac{L_m^2}{L_{sta}}\right)} \end{cases} \tag{26}$$

Among them: $K_r = \frac{K_s}{100}$.

III. DRNN CONTROL BASED DIFG WIND POWER SYSTEM

A. PROBLEM DESCRIPTION

Conventional DFIG systems are usually controlled using conventional PI controllers with simple characteristics. However, there are some difficulties in this control method, such as the dependence on system parameters and the lack of adaptive capability to the outside world. To improve the dynamic performance of DFIG, this paper proposes a modified recurrent neural network (CLR-DRNN) method for automatically adjusting the gain of the PI regulator while ensuring the independence of the generator settings.

PI regulators usually contain two gains: proportional gain (K_P) and integral gain (K_I). These gains are used to weight the accumulated values of current and past errors and input the results into the control system. The control concept of a standard PI regulator is shown below:

$$u(t) = K_{Pr} \cdot e(t) + K_{Ir} \cdot \int_0^t e(t) \cdot dt \tag{27}$$

However, in this study, a modified recurrent neural network method (CLR-DRNN) is proposed in order to improve the control performance of DFIG. This method is able to automatically adjust the gain of the PI regulator and ensure the independence of the generator settings. By weighting and calculating the accumulation and sum of error values, we can achieve optimization of the PI regulator. This improved control method aims to improve the dynamic performance of the DFIG system with better adaptive capabilities.

B. PRINCIPLE AND STRUCTURE OF BP NEURAL NETWORK AND DRNN NEURAL NETWORK

DRNN is similar to BP neural network, which consists of input, hidden and output layers, and the number of neurons in its hidden layer is determined by an empirical formula. The structure of DRNN neural network is shown in Fig. 2 and Fig. 3.

In DRNN, the input layer unit receives the input signal, and the implied layer receives the input from the input layer and the self-feedback signal, which is passed to the output layer after the excitation function to complete the forward propagation. Then, according to the error between the output result of the output layer and the desired value, backward propagation is performed and the network connection weights are dynamically adjusted so that the result of the output layer gradually approaches the desired value. In this way, DRNN can continuously optimize itself to achieve more accurate output.

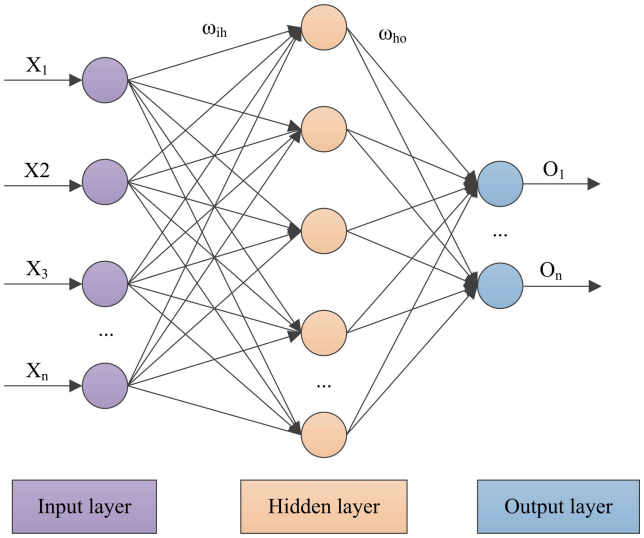

FIGURE 2. Schematic diagram of BP neural network.

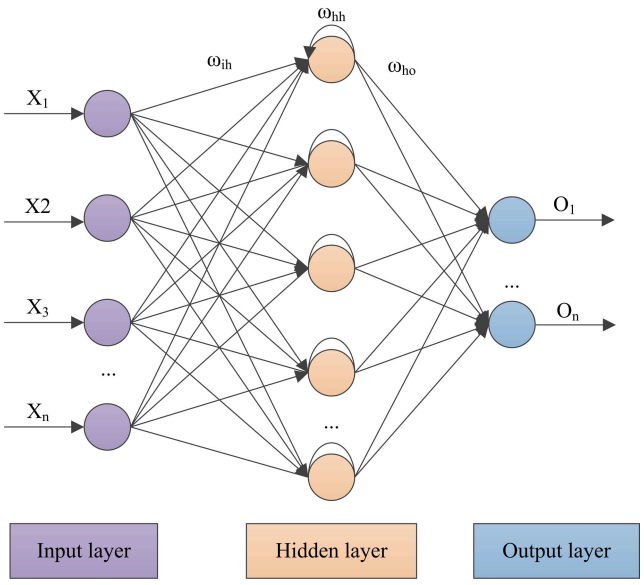

FIGURE 3. Schematic diagram of DRNN neural network.

Incremental PI control algorithm output expression:

$$u(k) = u(k-1) + K_p[e(k) - e(k-1)] + K_I e(k) \tag{28}$$

where $e(k)$ and $e(k-1)$ are the system errors collected by the controller for the last two times, respectively; $u(k)$ is the

controller output at k moments; K_p and K_I are the controller gain parameters. $e(k)$, $e(k)-e(k-1)$ and $u(k-1)$ are selected as the k-time input signal $X(k)$ of DRNN; the input $Z_h^{(2)}$ and output $A_h^{(2)}$ of each neuron in the hidden layer are:

$$\begin{cases} Z_h^{(2)}(k) = \sum_{i=1}^{3} \omega_{ih}^{(1)} X_i^{(1)}(k) + \omega_{hh}^{(1)} A_h^{(2)}(k-1) \\ A_h^{(2)}(k) = \sigma\left[Z_h^{(2)}(k)\right] \end{cases} \tag{29}$$

where ω_{ih} is the weight between each neuron in the input layer connected to the hidden layer; ω_{hh} is the weight of the neuron connected by self-feedback in the hidden layer $\sigma(x)$ is the excitation function of the hidden layer, where the hyperbolic tangent function is chosen and its expression is as follows:

$$\sigma(x) = \frac{e^x - e^{-x}}{e^x + e^{-x}} \tag{30}$$

The input $Z_o^{(3)}$ and output $A_0^{(3)}$ of each neuron in the output layer are:

$$\begin{cases} Z_o^{(3)}(k) = \sum_{h=1}^{5} \omega_{ho}^{(2)} A_h^{(2)}(k) \\ A_0^{(3)}(k) = g\left[Z_0^{(3)}(k)\right] \end{cases} \tag{31}$$

where ω_{ho} is the weight between each neuron in the output layer of the implicit layer connection; the output layer output is the controller gain parameters K_p and K_1, corresponding to:

$$\begin{cases} K_p = A_1^{(3)}(k) \\ K_1 = A_2^{(3)}(k) \end{cases} \tag{32}$$

Since the gain parameters are non-negative, the output layer excitation function is selected as a non-negative Sigmoid function with the following expressions:

$$g(x) = \frac{e^x}{e^x + e^{-x}} \tag{33}$$

The gain parameters required by the controller can be obtained by the forward propagation process described above. Subsequently, the output of the controller is calculated using equation (33) to influence the PI controller so that the DFIG produces an appropriate response. The learning process of the DRNN is based on a back-propagation algorithm that propagates the error signal back along the forward propagation path. This adjustment of the weight values between neurons leads to a continuous reduction of the system error. The performance exponential function of the system is defined as follows:

$$J(k) = \frac{1}{2}[r(k) - y(k)]^2 \tag{34}$$

where $r(k)$ is the desired value of the system, and $y(k)$ is the actual value. For the DFIG control system in this paper, $r(k)$ is the desired value of the speed or torque loop change controller, and $y(k)$ is the actual DFIG speed or torque. The gradient descent method is used to adjust the network weight values, and the adjustment formula is as follows:

$$\Delta\omega(k) = -\eta \frac{\partial J(k)}{\partial \omega(k)} + \alpha \Delta\omega(k-1) \tag{35}$$

where η is the learning rate; α is the inertia factor that makes the search converge quickly. According to the above equation, the weight adjustment formula between each neuron in the output layer to the hidden layer can be obtained as follows:

$$\Delta\omega_{ho}^{(2)}(k) = -\eta e(k) \frac{\partial y(k)}{\partial \Delta u(k)} \frac{\partial \Delta u(k)}{\partial A_o^{(3)}(k)} \cdot \times g'[Z_o^{(3)}(k)] A_h^{(2)}(k) + \alpha \Delta\omega_{ho}^{(2)}(k-1) \tag{36}$$

where $\frac{\partial y(k)}{\partial \Delta u(k)}$ is not known, here we adopt an approximate calculation method, using the symbolic function sgn(.) to approximate its replacement, and the resulting calculation inaccuracy can be compensated by adjusting the learning rate. Then the term can be expressed as follows:

$$\operatorname{sgn}\left(\frac{\partial y(k)}{\partial \Delta u(k)}\right) = \begin{cases} 1 & \frac{\partial y(k)}{\partial \Delta u(k)} \geq 0 \\ -1 & \frac{\partial y(k)}{\partial \Delta u(k)} < 0 \end{cases} \tag{37}$$

Similarly, the adjustment formula for the weight $\omega_{ih}^{(1)}$ among the neurons in the hidden layer to the output layer and the adjustment formula for the weight $\omega_{hh}^{(1)}$ among the neurons in the self-feedback loop in the hidden layer can be obtained as follows, respectively:

$$\Delta\omega_{ih}^{(1)}(k) = -\eta e(k) \operatorname{sgn}\left(\frac{\partial y(k)}{\partial \Delta u(k)}\right) \cdot \times \sigma'[Z_h^{(2)}(k)] X_i^{(1)}(k) \delta(k) + \alpha \Delta\omega_{ih}^{(1)}(k-1) \tag{38}$$

$$\Delta\omega_{hh}^{(1)}(k) = -\eta e(k) \operatorname{sgn}\left(\frac{\partial y(k)}{\partial \Delta u(k)}\right) \cdot \times \sigma[Z_h^{(2)}(k)] A_h^{(2)}(k-1) \delta(k) + \alpha \Delta\omega_{hh}^{(2)}(k-1) \tag{39}$$

where: $\delta(k) = \sum_{o=1}^{3} \left(\frac{\partial \Delta u(k)}{\partial A_o^{(3)}(k)} g'[Z_o^{(3)}(k)]\right) \omega_{ho^{(2)}(k)}$

C. LEARNING RATE ADAPTIVE OPTIMIZATION

The effectiveness and convergence speed of the DRNN learning algorithm are directly influenced by the learning rate η. A larger learning rate can accelerate the convergence speed of the neural network, but it may lead to weight oscillation and affect the controller performance, which is not conducive to the stable operation of the DFIG system. Although a smaller learning rate can avoid this situation, it will also reduce the convergence speed of DRNN and fail to adjust the controller parameters in time when dealing with complex environments. Therefore, an adaptive learning rate method

is proposed to balance the stability and fast response capability of the system. The adjustment equation is shown as follows:

$$\boldsymbol{\eta}(k) = \begin{cases} \boldsymbol{\eta}(k-1) + |\mathrm{e(k)}|/\boldsymbol{\beta} & \left(y^k \times y^{k-1}\right) > 0 \\ \boldsymbol{\eta}(k-1) \times \boldsymbol{\gamma} & \left(y^k \times y^{k-1}\right) < 0 \end{cases} \tag{40}$$

In the above equation, y^k denotes $\mathrm{sgn}\left(\frac{\partial y(k)}{\partial \Delta u(k)}\right)$ and y^k represents the directional information of the system output to the control input change at moment k. If the direction of change from moment k to moment $k-1$ is the same, the learning rate increases $|\mathrm{e(k)}|/\boldsymbol{\beta}$, where $\boldsymbol{\beta}$ is the scaling factor; conversely, it decreases $\boldsymbol{\gamma}$ times, and $\boldsymbol{\gamma}$ is a positive number less than 1, which should not be too small to avoid gradient disappearance. However, adopting the adaptive learning rate adjustment formula may result in the learning rate eventually becoming smaller and the weights cannot be adjusted in time when dealing with sudden changes in speed. Therefore, the following equation is adopted to correct the learning rate:

$$\eta(k) = \eta_0 e(k) - e(k-1) > \Delta\omega \tag{41}$$

where η_0 is the corrected learning rate, and equation (49) is activated to correct the learning rate when the error value at time k minus the error value at time $k-1$ is greater than the threshold value $\Delta\omega$.

IV. SIMULATION AND VALIDATION OF DRNN ALGORITHM BASED ON IMPROVED LEARNING RATE

A. IMPLEMENTATION OF DFIG ROTOR-SIDE PI CONTROL BASED ON BP AND IMPROVED DRNN NEURAL NETWORK ALGORITHM

BP neural networks and DRNN neural networks are widely used in pattern recognition and classification problems, and are also effective means of application in PI controllers. Specifically, neural networks can adjust the parameters of PI controllers by monitoring the error of the feedback signal and the desired output signal to improve the performance and response speed of the controller. The training process of neural networks usually consists of two stages: forward propagation and backward propagation. In forward propagation, the network passes the input signal to the output layer for error calculation, while in backward propagation, the error is fed back to the input layer and a gradient descent algorithm is used to adjust the weights and bias values of each neuron to minimize the error.

For the DFIG system as the controlled object, the K_P and K_I parameters of the PI controller can be determined by inputting the actual output value y(t), the target signal rin(t) and the error e(t) into the BP and DRNN neural networks. Finally, these parameters are passed to the PI controller to enable it to control the controlled object more accurately and thus improve the control effect. The following figures show the whole process (Figure 4 and Figure 5).

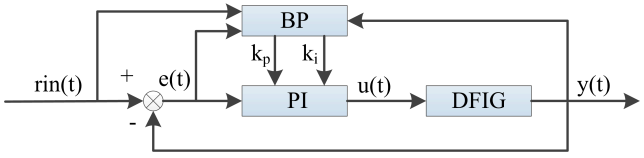

FIGURE 4. Schematic diagram of PI control structure based on BP neural network.

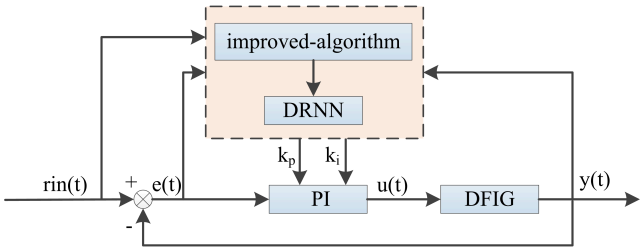

FIGURE 5. Schematic diagram of DRNN-based neural network PI control structure.

B. NEURAL NETWORK FLOW CHART

The algorithm flow is as follows:

(1) Determine the DRNN neural network structure, initialize the weight values, select the appropriate learning rate and momentum factor, so that $k = 1$;
(2) Sample the input $r(k)$ and output $y(k)$ at time k, and calculate the deviation $e(k)$;
(3) Input $e(k)$, $e(k) - e(k-1)$ and $u(k-1)$ into the DRNN and calculate the output quantities K_p and K_1;
(4) Calculate the control output $u(k)$ at that moment according to equation (3);
(5) calculate the learning rate at the current moment, and adjust the network weight coefficients according to the back propagation formula to achieve adaptive control;
(6) Let $k = k + 1$ and return to step (2).

The neural network algorithm flow is shown in Figure 6.

C. COMPARISON OF ORIGINAL PI CONTROL, BP CONTROL, DRNN CONTROL, AND IMPROVED DRNN CONTROL

To verify the effect of the improved DRNN algorithm on the PI controller, we built a MATLAB/Simulink simulation model and conducted simulation experiments to compare and verify the improved DRNN algorithm to improve the effect of the PI controller. Figure 7 shows the controlled object y(t), assuming that y(t) is a continuous signal from 0 to 10 seconds with a step at 1 second, from y(t) equal to 0 to 1, and remains constant for the following 9 seconds. By using the original PI controller to track the controlled quantity, the output signal of the original PI controller reaches the output value of the controlled object at 1.6 seconds, but oscillation occurs afterwards, with a maximum oscillation amplitude of about 1.4 at

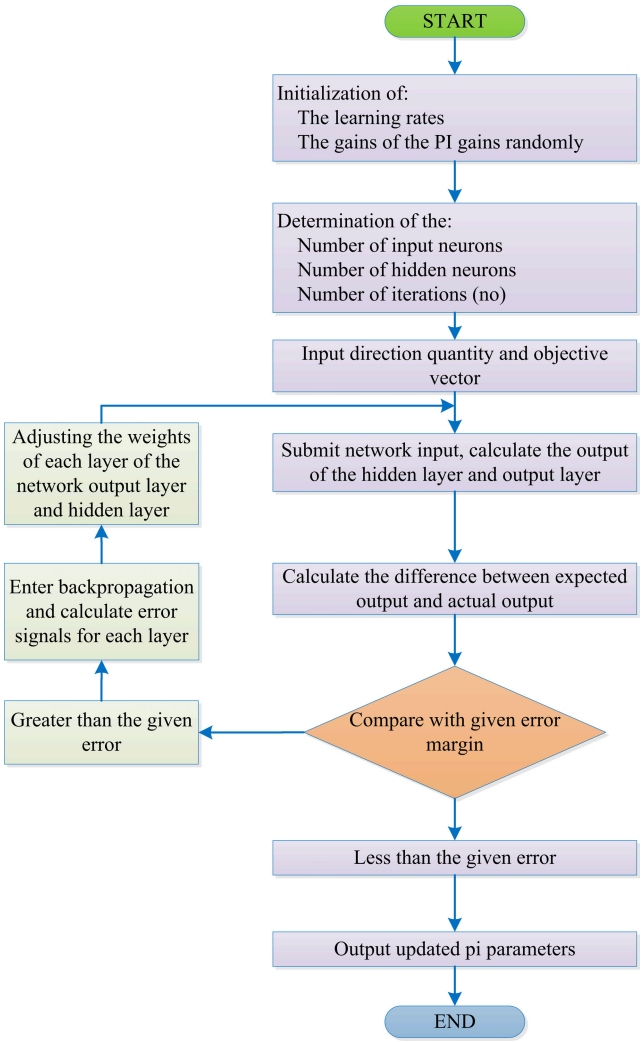

FIGURE 6. Neural network flow chart.

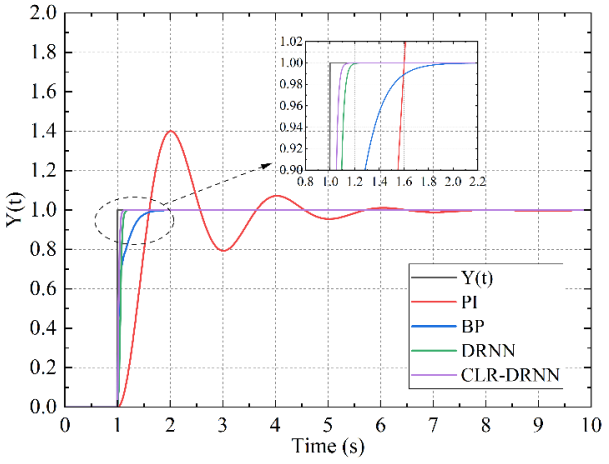

FIGURE 7. Neural network tracking step function effect graph.

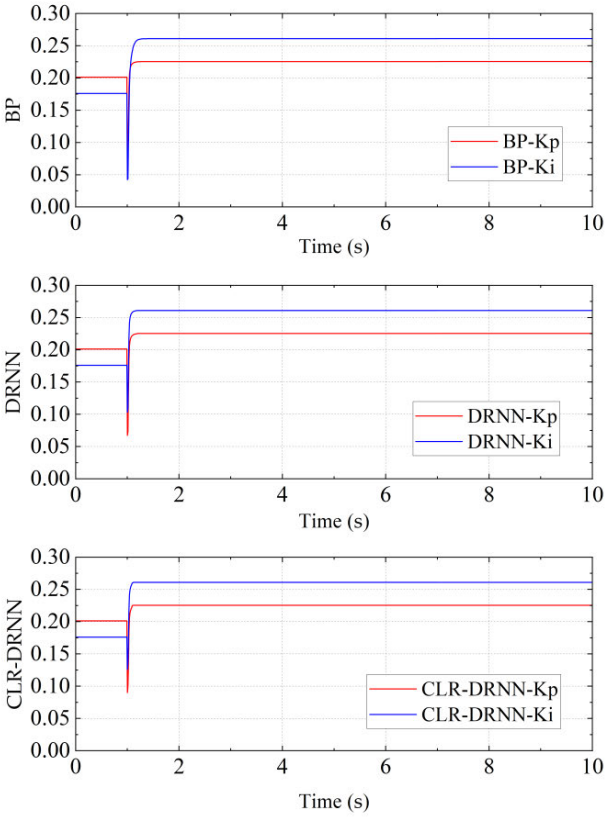

FIGURE 8. PI parameter change diagram.

2 seconds and an overshoot of about 40%, and it takes about 7.6 seconds to track the controlled object. It can be seen that the original PI controller control effect is not ideal.

As seen in Figure 7, the control effect of the PI controller has been significantly improved by the improved DRNN neural network.

The output of the PI controller based on BP neural network tracked the control amount in about 2.2 seconds, while the output of the PI controller based on DRNN neural network and the improved DRNN neural network tracked the control amount in about 1.2 seconds. Also, the output overshoot of the PI controller based on the neural network algorithm is almost zero. Figure 8 shows the K_P, K_I parameters of the BP controller optimized based on BP neural network, DRNN neural network and the modified DRNN neural network. As can be seen from Figure 8, the oscillation amplitudes of the K_P and K_I parameters of the BP neural network-based PI controller are 0.1754 and 0.22209, respectively, with a response time of about 0.2 seconds; the oscillation amplitudes of the K_P and K_I parameters of the DRNN neural network-based PI controller are 0.1654 and 0.1609, respectively, with a response time of about 0.15 seconds; the response time based on the improved The oscillation amplitudes of K_P and K_I parameters of the PI controller based on the modified DRNN neural network are 0.1550 and 0.1409, respectively, with a response time of about 0.15 seconds.

The experiments effectively verify the effectiveness of the optimized PI controller based on the neural network algorithm. Compared with the original PI controller, the

neural network based optimized PI controller has significant improvement in response time, control effect and overshoot amount.

V. SIMULATION AND RESULTS

A. APPLICATION OF IMPROVED DRNN NEURAL NETWORK TO DFIG WIND POWER SYSTEM

Figure 9 shows the design of the control process based on the improved DRNN neural network optimization for the DFIG rotor-side PI controller. In the DFIG-based wind power system, the voltage stability is related to the reactive power deviation $|Q_s - Q_s^*|$ and the frequency stability is related to the rotor angular speed error $|\omega_r - \omega_r^*|$. Different control parameters will have an impact on the control effect of the system. The traditional PI controller parameters are based on the global optimal solution, which usually requires a combination of several aspects and therefore cannot represent the best control effect at a certain moment. In this paper, we propose a method to improve the PI controller using a modified recurrent neural network (CLR-DRNN).

First, the optimal rotor speed, real-time speed, optimal reactive power and real-time reactive power are input into the neural network intelligent algorithm module to determine the optimal parameters K_P and K_I for the power loop by the neural network intelligent optimization algorithm. then, the optimal current value and the actual current value are input into the neural network intelligent optimization algorithm module to determine the optimal parameters K_P and K_I for the current loop.

In this design, we adopted some strategies to improve the stability and regulation speed of the system. For the power loop regulation, we chose the traditional PI regulation method to ensure the stability of the system. As for the current loop regulation, we used an intelligent optimization algorithm to adjust it dynamically to improve the accuracy of regulation. For this purpose, we designed a neural network model with a 3-5-2 structure for implementing the current loop regulation. With these measures, we expect the system to perform power and current regulation more stably and efficiently.

B. SYSTEM PARAMETER SETTING

According to the operation and control principle of doubly-fed wind power generation system, MATLAB2022a software is used to build the overall simulation model of doubly-fed wind power generation system.

The main parameters of the DFIG system model are shown in Table 1. The simulated DFIG works at a fixed pitch, the pitch angle is $\beta = 0°$, the rated wind speed is 11.2m/s, the cut-in wind speed is 3/s, the cut-out wind speed is 25m/s, the optimal blade tip speed ratio b is λ_{opt}, and the maximum wind energy utilization coefficient $C_{p\max}$ is 0.4412.

In MATLAB/Simulink platform to build a combined wind speed model as shown in Figure 10, now set the simulation parameters of the wind speed model as follows:

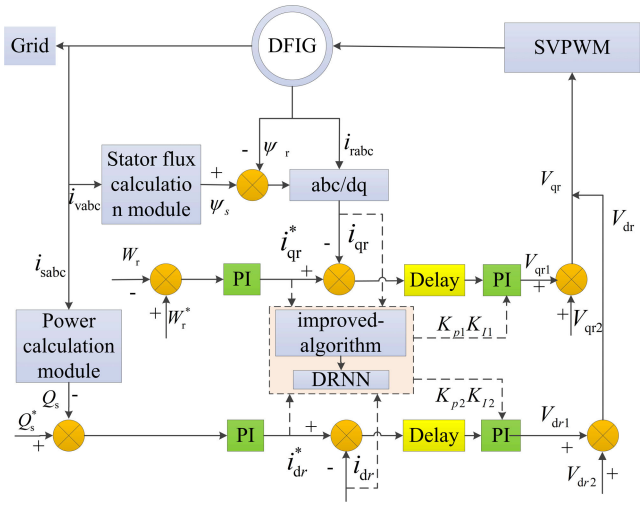

FIGURE 9. RSC parameter optimization structure of DFIG-based wind power system under intelligent algorithm.

TABLE 1. Parameters of wind power plant system components.

Symbol	Parameters	Values
R_w	Radius of blade	44 m
T	Coefficient of multiplier	100
J	Total moment of inertia	90 kg.m2
D	Damping friction factor	0.1 N.m.s
P	DFIG rated power	2 Mw
L_{si}	Stator leakage inductance	0.087 uh
R_{res}	Rotor resistance	0.0261 mh
R_{ind}	Rotor leakage inductance	0.783 uh
L_m	Mutual inductance	0.0025 mh
V_{dc}	Stator line to line voltage	1200 v
C	DC-link capacitance	1500 μF
R_f	Resistor of the filter	10 Ω
L_f	Inductance of the filter	0.05 h
p	Pole pair	2

the simulation time is 10s, at the moment of 0 the basic wind speed is 4m/s, the duration is 2 seconds; at the moment of 2 seconds, the wind speed changes abruptly, at this time the basic wind speed becomes 8m/s, the duration is 4 seconds; at the moment of 6 seconds, the basic wind speed at 6 seconds, the basic wind speed becomes 10m/s and the duration is 4 seconds. The step wind speed is obtained by simulation.

C. SIMULATION EXPERIMENT RESULTS

To demonstrate the superiority of control using the neural network algorithm, four parameters reflecting the quality of RSC control performance were selected for comparison in this study, including wind energy conversion efficiency C_p, active power P, reactive power Q, and rotor angular velocity ω.

As shown in Figure 11, the graph reflects the fluctuation of the maximum wind energy utilization factor. Based on

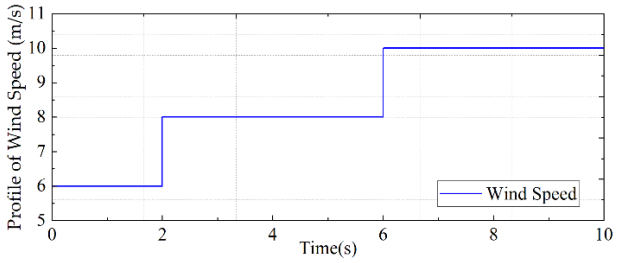

FIGURE 10. PI parameter change diagram.

the DFIG system parameters in Table 1 and the relevant calculation equations, we know that the wind energy utilization coefficient of the DFIG turbine simulated in this time is about 0.4412. It can be observed from Figure 11 that a step in wind speed occurs at 2 s. Based on the four control methods, PI, BP, DRNN and CLR-DRNN, the overshoot of DFIG wind energy utilization coefficient is 0.1192, 0.0662, 0.0552 and 0.0162, respectively, and the overshoot percentages are about 27.01%, 15.00%, 12.51% and 3.67%, and the convergence times are 2.56, 1.35, 0.25, and 0.16 seconds. At 6 seconds when the wind speed steps again, the overshoot of DFIG wind energy utilization coefficient is 0.1562, 0.0902, 0.0652 and 0.0252 based on four control methods, PI, BP, DRNN and CLR-DRNN, with overshoot percentages of about 35.40%, 20.44%, 14.78% and 5.71%, with convergence times of 2.55, 1.50, 0.30, and 0.18 seconds, respectively.

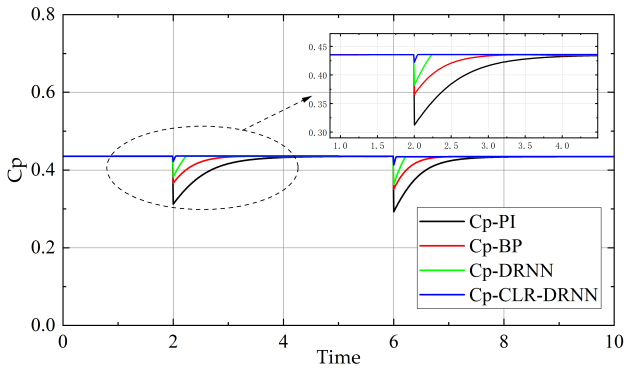

FIGURE 11. Maximum wind energy utilization factor Cp.

As shown in Figure 12, this figure demonstrates the active power fluctuation of the DFIG. It can be observed that the wind speed changes abruptly at 2 seconds, and the convergence times of the active power curves are 2.55 seconds, 2.20 seconds, 1.80 seconds and 1.78 seconds for the DFIG with four different control methods. At 6 seconds, the wind speed changed abruptly again, while the convergence times of the corresponding DFIG active power curves were 2.65 seconds, 2.25 seconds, 1.85 seconds and 1.80 seconds, respectively. From the DFIG active power curves, it can be seen that the DFIG systems based on the DRNN and CLR-DRNN control methods are significantly better than the DFIG systems based on the PI and BP control methods. In addition, the active power curve of the DFIG based on the CLR-DRNN control method always lies above the curve of the DFIG based on the DRNN control method.

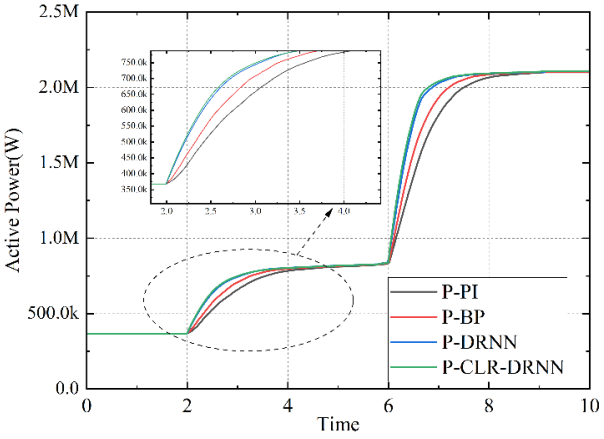

FIGURE 12. Active power fluctuation.

As shown in Figure 13, the graph illustrates the fluctuation of reactive power of DFIG. The wind speed changes abruptly at 2 seconds, and the overshoot of the DFIG wind energy utilization factor is 14.5 KW, 7.2 KW, 4.5 KW and 3.0 KW with convergence times of 0.65, 0.40, 0.25 and 0.15 seconds, respectively, using the four control methods PI, BP, DRNN and CLR-DRNN. At 6 seconds, the wind speed changed abruptly again, and the same four control methods were used at this time. The corresponding overshoot of the DFIG wind energy utilization factor was 24.5 KW, 17.2 KW, 8.5 KW and 6.0 KW, and the convergence times were 0.90 s, 0.60 s, 0.35 s and 0.20 s, respectively.

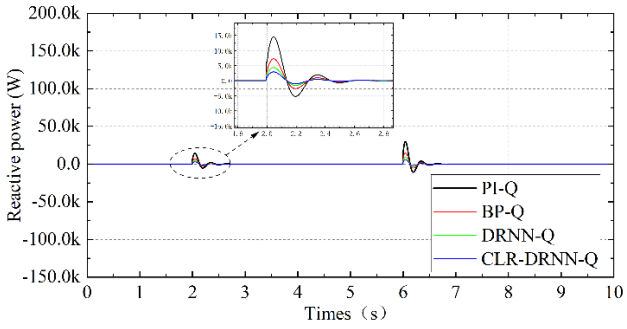

FIGURE 13. Reactive power fluctuation.

As shown in Figure 12, the graph demonstrates the rotor speed fluctuation of DFIG. The wind speed changes abruptly at 2s and the convergence times of the rotor speed fluctuation curves of DFIG are 2.65s, 2.25s, 2.10s and 2.05s, respectively. At 6 seconds, the wind speed changed abruptly again, and the same four control methods were used at this time, while the corresponding convergence times of the DFIG rotor speed

fluctuation curves were 2.85, 2.35, 2.20 and 2.15 seconds, respectively. From the DFIG rotor speed fluctuation curves, it can be seen that the DFIG system based on the DRNN and CLR-DRNN control methods is significantly better than the DFIG system based on the PI and BP control methods. In addition, the rotor speed fluctuation curve of the DFIG based on the CLR-DRNN control method always lies above the curve of the DFIG based on the DRNN control method.

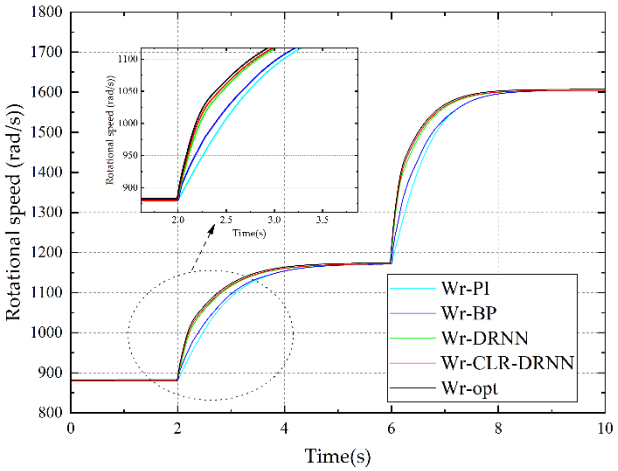

FIGURE 14. Rotor speed.

D. ROTOR CURRENT AND STATOR CURRENT

By learning a large amount of data and samples, the CLR-DRNN control module can establish complex nonlinear mapping relationships. This allows it to better capture the correlation between currents and control strategies and provide more accurate control results. In addition, the CLR-DRNN control module has the ability to handle input data noise and disturbances, thus enhancing the robustness of the control system.

Figure 15 illustrates the DFIG rotor current fluctuation based on CLR-DRNN control. the CLR-DRNN control module is able to receive the rotor current input and learn the characteristics and patterns of the current to better understand the dynamic changes of the current and to predict and control it. Changes in rotor current are critical input signals for the CLR-DRNN control module and require real-time response for appropriate control strategy adjustment. With the cyclic structure, the CLR-DRNN control module is able to capture the time dependence of the current and respond quickly.

Figure 15 shows that the CLR-DRNN control module achieves a smooth and rapid control effect on the rotor current at the 2 and 6 second moments when the step in wind speed occurs. This is due to its ability to automatically learn the current characteristics and adapt them to the actual situation. the CLR-DRNN control module has the capability of adaptive learning and optimization, and by continuously iterating and adjusting the network parameters, it can improve the control performance and achieve a more optimized DFIG control.

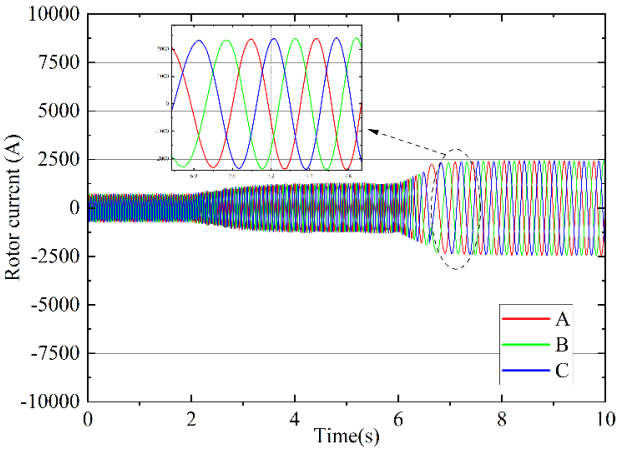

FIGURE 15. Rotor current.

Figure 16 presents the fluctuation of DFIG stator current based on CLR-DRNN control. the CLR-DRNN control module has the ability of adaptive learning and optimization to improve the control performance by continuously adjusting the network parameters and iterative optimization. It is able to learn the characteristics of the current autonomously and make adaptive adjustments according to the actual situation to achieve a more optimized DFIG control effect.

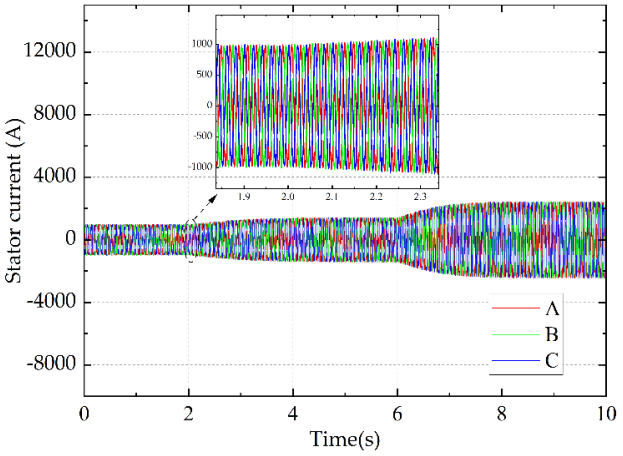

FIGURE 16. Stator current.

According to Figure 16, it can be observed that the CLR-DRNN control module successfully achieves smooth and rapid control of the stator current at the 2-second and 6-second moments when the step in wind speed occurs. This is due to the CLR-DRNN control module's feature of automatically learning the current characteristics and adaptively adjusting to the actual situation, allowing it to respond to current changes in a timely manner and achieve high precision control. These advantages make the CLR-DRNN-based DFIG control promising in practical applications, providing stable and efficient operation for wind power systems.

VI. CONCLUSION

In this paper, we present an in-depth analysis of the problems of DFIG wind power system control. By reviewing the literature and conducting research, we find that neural network algorithms have significant advantages in regulating control parameters. First, we establish a mathematical model and simulation model of DFIG and propose a method to improve DFIG control using diagonal recurrent neural networks (DRNN). Given that the learning rate of DRNN algorithm affects the control effect, accuracy, response time and overshoot, we improve the learning rate of DRNN algorithm and propose a diagonal recurrent neural network with improved learning rate (CLR-DRNN) for dynamic parameter tuning of DFIG wind power system.

In terms of tracking step function, we compare the traditional PI control method and the PI control method based on BP, DRNN, and CLR-DRNN, and verify the effectiveness of the proposed method by simulation experimental results, including the overshoot amount and response time. Finally, we apply several control methods to the DFIG control system and find that the DFIG system based on the CLR-DRNN control method shows better performance in terms of wind energy utilization factor, active power, reactive power and rotor speed. Compared with other control methods, the CLR-DRNN control method has lower overshoot, shorter convergence time and more stable curve performance.

In summary, the CLR-DRNN-based DFIG control has great potential to improve system performance and can provide strong support for stable and efficient operation of wind power generation systems. This study provides a useful reference for the improvement and optimization of DFIG control algorithm and provides a basis for future related research and practice.

REFERENCES

[1] S. Mensou, A. Essadki, T. Nasser, B. B. Idrissi, and L. Ben Tarla, "Dspace DS1104 implementation of a robust nonlinear controller applied for DFIG driven by wind turbine," *Renew. Energy*, vol. 147, pp. 1759–1771, Mar. 2020.

[2] H. D. Song and X. Y. Dong, "Current situation and development trend of wind power generation technology," *Electr. Eng. Elect.*, to be published.

[3] Z. Y. Song, X. F. Wang, Y. F. Teng, L. H. Ning, and Q. Zhang, "Overview of control technology for variable-speed constant-frequency wind turbine generators," *Power Syst. Autom.*, vol. 34, no. 10, pp. 8–17, 2010.

[4] V. Yaramasu and B. Wu, *Model Predictive Control of Wind Energy Conversion Systems*. Hoboken, NJ, USA: Wiley, 2016.

[5] S. Boubzizi, H. Abid, A. El Hajjaji, and M. Chaabane, "Comparative study of three types of controllers for DFIG in wind energy conversion system," *Protection Control Modern Power Syst.*, vol. 3, no. 1, pp. 1–12, Dec. 2018.

[6] E. Chetouani, Y. Errami, A. Obbadi, and S. Sahnoun, "Optimal tuning of PI controllers using adaptive particle swarm optimization for doubly-fed induction generator connected to the grid during a voltage dip," *Bull. Electr. Eng. Informat.*, vol. 10, no. 5, pp. 2367–2376, Oct. 2021.

[7] M. A. Soomro, Z. A. Memon, M. Kumar, and M. H. Baloch, "Wind energy integration: Dynamic modeling and control of DFIG based on super twisting fractional order terminal sliding mode controller," *Energy Rep.*, vol. 7, pp. 6031–6043, Nov. 2021.

[8] K. Deb, *Optimization for Engineering Design: Algorithms and Examples*. New Delhi, India: PHI Learning Pvt. Ltd., 2012.

[9] A. Zakaria, F. B. Ismail, M. S. H. Lipu, and M. A. Hannan, "Uncertainty models for stochastic optimization in renewable energy applications," *Renew. Energy*, vol. 145, pp. 1543–1571, Jan. 2020.

[10] N. Panda and S. K. Majhi, "Effectiveness of swarm-based metaheuristic algorithm in data classification using pi-sigma higher order neural network," in *Progress in Advanced Computing and Intelligent Engineering: Proceedings of ICACIE*, vol. 2, vol. 2. Singapore: Springer, 2021, pp. 77–88.

[11] T. T. Li, "Research on hyperparametric optimization problem based on improved particle swarm algorithm," Ph.D. dissertation, Xi'an Univ. Electron. Sci. Technol., Xi'an, China, 2020.

[12] E. Chetouani, Y. Errami, A. Obbadi, and S. Sahnoun, "Self-adapting PI controller for grid-connected DFIG wind turbines based on recurrent neural network optimization control under unbalanced grid faults," *Electr. Power Syst. Res.*, vol. 214, Jan. 2023, Art. no. 108829.

[13] G. Chen, T. T. Pham, and N. M. Boustany, "Introduction to fuzzy sets, fuzzy logic, and fuzzy control systems," *Appl. Mech. Rev.*, vol. 54, no. 6, pp. B102–B103, 2001.

[14] B. Chen, J. Duan, J. Wang, B. Qin, and Z. Li, "Frequency regulation control strategy for combined wind-storage system considering full wind speed," in *Proc. 12th Int. Conf. Power Energy Syst. (ICPES)*, Dec. 2022, pp. 737–742.

[15] F. Zhou, L. Jin, and J. Dong, "A review of convolutional neural network research," *J. Comput. Sci.*, vol. 40, no. 6, pp. 1229–1251, 2017.

[16] R. Oliver, "Negative feedback in child NS-NNS conversation," *Stud. Second Lang. Acquisition*, vol. 17, no. 4, pp. 459–481, Dec. 1995.

[17] H. Rahmanifard and T. Plaksina, "Application of artificial intelligence techniques in the petroleum industry: A review," *Artif. Intell. Rev.*, vol. 52, no. 4, pp. 2295–2318, Dec. 2019.

[18] A. A. Yesudhas, Y. H. Joo, and S. R. Lee, "Reference model adaptive control scheme on PMVG-based WECS for MPPT under a real wind speed," *Energies*, vol. 15, no. 9, p. 3091, Apr. 2022.

[19] I. Yaichi, A. Semmah, and P. Wira, "Control of doubly fed induction generator with maximum power point tracking for variable speed wind energy conversion systems," *Periodica Polytechnica Electr. Eng. Comput. Sci.*, vol. 64, no. 1, pp. 87–96, Nov. 2019.

[20] J. Yosinski, J. Clune, and Y. Bengio, "How transferable are features in deep neural networks?" in *Proc. Adv. Neural Inf. Process. Syst.*, vol. 27, 2014.

[21] R. D. Beer and J. C. Gallagher, "Evolving dynamical neural networks for adaptive behavior," *Adapt. Behav.*, vol. 1, no. 1, pp. 91–122, Jun. 1992.

[22] S. Li, Y. Zhang, and L. Jin, "Kinematic control of redundant manipulators using neural networks," *IEEE Trans. Neural Netw. Learn. Syst.*, vol. 28, no. 10, pp. 2243–2254, Oct. 2017.

[23] J. Adler and O. Öktem, "Solving ill-posed inverse problems using iterative deep neural networks," *Inverse Problems*, vol. 33, no. 12, Dec. 2017, Art. no. 124007.

[24] A. Mackey, R. Oliver, and J. Leeman, "Interactional input and the incorporation of feedback: An exploration of NS-NNS and NNS-NNS adult and child dyads," *Lang. Learn.*, vol. 53, no. 1, pp. 35–66, Mar. 2003.

[25] S. Saha and G. P. S. Raghava, "Prediction of continuous B-cell epitopes in an antigen using recurrent neural network," *Proteins, Struct., Function, Bioinf.*, vol. 65, no. 1, pp. 40–48, Aug. 2006.

[26] D. You, X. Gao, and S. Katayama, "WPD-PCA-based laser welding process monitoring and defects diagnosis by using FNN and SVM," *IEEE Trans. Ind. Electron.*, vol. 62, no. 1, pp. 628–636, Jan. 2015.

[27] J. Koutnik, K. Greff, and F. Gomez, "A clockwork RNN," in *Proc. Int. Conf. Mach. Learn.*, 2014, pp. 1863–1871.

[28] H. Shao and G. Zheng, "A new BP algorithm with adaptive momentum for FNNs training," in *Proc. WRI Global Congr. Intell. Syst.*, vol. 4, May 2009, pp. 16–20.

[29] H. Benbouhenni, "Two-level DPC strategy based on FNN algorithm of DFIG-DRWT systems using two-level hysteresis controllers for reactive and active powers," *Renew. Energy Res. Appl.*, vol. 2, no. 1, pp. 137–146, 2021.

[30] Z. Y. Xue, K. S. Xiahou, M. S. Li, T. Y. Ji, and Q. H. Wu, "Diagnosis of multiple open-circuit switch faults based on long short-term memory network for DFIG-based wind turbine systems," *IEEE J. Emerg. Sel. Topics Power Electron.*, vol. 8, no. 3, pp. 2600–2610, Sep. 2020.

[31] Y. Chu, J. Fei, and S. Hou, "Adaptive global sliding-mode control for dynamic systems using double hidden layer recurrent neural network structure," *IEEE Trans. Neural Netw. Learn. Syst.*, vol. 31, no. 4, pp. 1297–1309, Apr. 2020.

[32] S. Zhao, D. Zhao, and C. Zhi, "Study of PI control method for electromechanical actuators based on improved DRNN," *Microtechnology*, vol. 49, no. 12, p. 35, 2021.

[33] T. X. Wang, H. Y. Ma, and M. H. Nie, "Study of BP neural network PID speed control method for permanent magnet synchronous motor for elevator," *J. Electrotechnol.*, vol. 2015, no. S1, pp. 43–47, 2015.
[34] X. Li, Y. Liu, and X. Ye, "Single-neuron PID-based decoupling control of permanent magnet synchronous motor," *Power Electron. Technol.*, vol. 47, no. 9, pp. 58–59, 2013.
[35] Y. Zahraoui, I. Alhamrouni, S. Mekhilef, M. R. B. Khan, M. Seyedmahmoudian, A. Stojcevski, and B. Horan, "Energy management system in microgrids: A comprehensive review," *Sustainability*, vol. 13, no. 19, Sep. 2021, Art. no. 10492.
[36] S. Labdai, N. Bounar, A. Boulkroune, B. Hemici, and L. Nezli, "Artificial neural network-based adaptive control for a DFIG-based WECS," *ISA Trans.*, vol. 128, pp. 171–180, Sep. 2022.
[37] K. K. Jaladi and K. S. Sandhu, "Real-time simulator based hybrid control of DFIG-WES," *ISA Trans.*, vol. 93, pp. 325–340, Oct. 2019.
[38] X. W. Peng and R. D. Lorenz, "Development and application of a multi-agent control system for distributed generation," *Electr. Power Syst. Res.*, to be published.

TAO CHENG was born in Anhui, China, in April 1996. He received the Graduate degree from the School of Electrical Engineering, Shijiazhuang Railway University, China, in 2020. He is currently pursuing the master's degree in engineering with the School of Electricity, Xinjiang University, China.

His current research interest includes wind power stability analysis.

JIAHUI WU was born in Xuzhou, Jiangsu, in 1988.

She is currently with the School of Electrical Engineering, Xinjiang University. Her main research interests include wind power grid-connected system stability research and complex energy system stability analysis and control.

HAIYUN WANG was born in 1973.

She is currently a Ph.D. Supervisor and a Professor. She is also with the School of Electricity, Xinjiang University. Her main research interest includes wind power grid-connected system stability.

HONGJUAN ZHENG was born in Yancheng, Jiangsu, in 1989.

She is currently an Assistant Engineer with Guodian Nanrui Technology Company Ltd., Nanjing, Jiangsu. Her main research interests include virtual power plant and demand response.